Probing Transport and Slow Relaxation in the Mass-Imbalanced Fermi-Hubbard Model

N. Darkwah Oppong,[1,2,3,*] G. Pasqualetti,[1,2,3] O. Bettermann,[1,2,3] P. Zechmann,[4,3] M. Knap,[4,3] I. Bloch,[1,2,3] and S. Fölling[1,2,3]

[1]*Ludwig-Maximilians-Universität, Schellingstraße 4, 80799 München, Germany*
[2]*Max-Planck-Institut für Quantenoptik, Hans-Kopfermann-Straße 1, 85748 Garching, Germany*
[3]*Munich Center for Quantum Science and Technology (MCQST), Schellingstraße 4, 80799 München, Germany*
[4]*Department of Physics and Institute for Advanced Study, Technical University of Munich, 85748 Garching, Germany*

(Received 24 November 2020; accepted 12 May 2022; published 16 August 2022)

Constraints in the dynamics of quantum many-body systems can dramatically alter transport properties and relaxation timescales even in the absence of static disorder. Here, we report on the observation of such constrained dynamics arising from the distinct mobility of two species in the one-dimensional mass-imbalanced Fermi-Hubbard model, realized with ultracold ytterbium atoms in a state-dependent optical lattice. By displacing the trap potential and monitoring the subsequent dynamical response of the system, we identify suppressed transport and slow relaxation with a strong dependence on the mass imbalance and interspecies interaction strength, consistent with eventual thermalization for long times. Our observations demonstrate the potential for quantum simulators to provide insights into unconventional relaxation dynamics arising from constraints.

DOI: 10.1103/PhysRevX.12.031026

Subject Areas: Atomic and Molecular Physics
Condensed Matter Physics
Statistical Physics

I. INTRODUCTION

The fundamental understanding of thermalization and its failure in isolated quantum many-body systems has seen remarkable progress in recent years, driven both by novel theoretical concepts [1–4] and emerging experimental platforms for quantum simulations such as ultracold atoms, trapped ions, and superconducting qubits [5–7]. The simplest approach to the problem is to posit the two distinct classes of ergodic and nonergodic dynamics. In the former case, fast relaxation to a local equilibrium is followed by slow thermalization of globally conserved quantities according to the laws of hydrodynamics [8–11]. By contrast, nonergodic dynamics can arise in systems with a large number of conserved quantities, as exemplified by many-body localization in strongly disordered quantum systems [12–15] that retain their memory of an initial state for arbitrarily long times [16–18].

Recent experimental and theoretical investigations of nonequilibrium dynamics in isolated quantum many-body systems, however, suggest considerable refinements to this classification. For instance, Rydberg quantum simulators have observed surprising oscillatory dynamics in the blockade regime [19,20], and the slow late-time dynamics of fractonic quantum matter with constrained excitations [21] is described by substantially modified hydrodynamic equations [22–24]. Furthermore, interacting mixtures of heavy and light particles [see Fig. 1(a)] have even been proposed to feature a dynamical type of many-body localization arising from the heavy particles acting as a form of disorder for the light ones [25–28]. Although subsequent studies have suggested that such heavy-light mixtures are ergodic and do thermalize at late times, the relaxation of initial nonequilibrium states is expected to be unconventionally slow [27,29–32]. This is a direct consequence of the strongly constrained motion in the presence of mass imbalance and interactions. However, since such heavy-light mixtures are particularly challenging to simulate with classical resources, these theoretical studies do not entirely agree on the exact properties of relaxation [30–32], which underlines the importance of experimental evidence. Crucially, this phenomenology connects to the general question of how dynamical constraints can introduce slow equilibration and nonergodicity in quantum many-body systems [33–38].

*n.darkwahoppong@lmu.de

In this work, we experimentally study the nonequilibrium dynamics of a heavy-light mixture with an ultracold quantum gas of ^{171}Yb atoms in an optical lattice. Our experiment realizes the strongly mass-imbalanced Fermi-Hubbard model in one dimension (1D), as illustrated in Fig. 1(a). In addition to the $^1S_0$ ground state (denoted $|g\rangle$), the alkaline-earth-like atom ^{171}Yb features the metastable $^3P_0$ excited state (denoted $|e\rangle$), often referred to as the clock state [39]. We harness a state-dependent optical lattice (SDL) [40] to introduce different timescales for the hopping of atoms in $|g\rangle$ and $|e\rangle$ taking on the role of light and heavy particles, respectively. Our system is harmonically confined, and we gradually displace the trap minimum with the help of an additional optical potential to probe the transport dynamics of the light species [see Fig. 1(b)]. Measuring the dynamics of the atomic cloud, we find relaxation at late times as a signature of ergodicity for all finite interaction parameters. However, this relaxation becomes slow compared to conventional timescales for strong interactions and large mass imbalance. Our observations cannot be explained by a mere reduction of the mobility for the heavy species alone, but rather they can be understood as emergent properties from the constrained many-body dynamics. Numerical simulations based on matrix-product states and exact diagonalization support our findings.

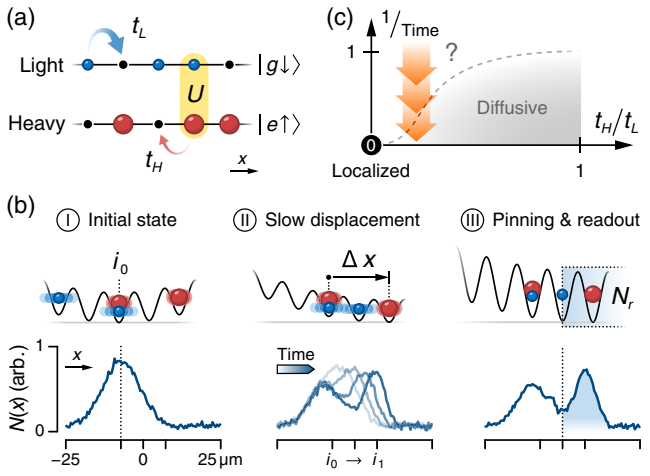

FIG. 1. Transport in the mass-imbalanced Fermi-Hubbard model. (a) Illustration of the mass-imbalanced Fermi-Hubbard model with on-site interaction U and hopping $t_L \gg t_H$ of the light (blue circles) and heavy (red circles) particles, respectively. We also show the atomic states relevant for the experimental implementation. (b) Schematic representation of the different steps in our transport measurement (top row) and integrated densities of the light atoms (bottom row) from experimental snapshots. (c) Scenario for the transient regime following a quench in the mass-imbalanced Fermi-Hubbard model for a variable inverse hold time (vertical axis). Here, the dashed line marks the crossover between unconventional relaxation dynamics at early times (question mark) and diffusion at late times. The orange arrows indicate a trajectory in the regime of our experiment.

II. EXPERIMENT

Our experiment begins with a Fermi gas of ^{171}Yb atoms in a balanced mixture of the two nuclear spins $|m_F = -1/2\rangle \equiv |\downarrow\rangle$ and $|m_F = +1/2\rangle \equiv |\uparrow\rangle$ in the ground state $|g\rangle$. In the initial optical dipole trap, we prepare a total of approximately 10^4 atoms at a temperature of $T \simeq 0.15T_F$, with T_F the Fermi temperature. The weakly interacting spin mixture is loaded from the optical dipole trap into the ground band of a two-axes, approximately $30E^m_{\mathrm{rec}}$ deep, state-independent lattice operated at the magic wavelength ($\lambda_m = 759.3$ nm) [41] and a $V_L = 6.9(3)E_{\mathrm{rec}}$ deep SDL ($\lambda = 671.5$ nm) along the third axis. Here, $E^m_{\mathrm{rec}} = h \times 2.0$ kHz and $E_{\mathrm{rec}} = h \times 2.6$ kHz are the recoil energies of the corresponding lattice photons. The atoms are nonuniformly distributed across the array of decoupled 1D systems (tubes) generated by the perpendicular state-independent lattices. We estimate that approximately 300 tubes are considerably filled with a mean atom number of $\mathcal{N} \simeq 18$ per spin state and standard deviation $\Delta\mathcal{N} \simeq 8$. In a typical tube, the atoms are spread over a system size of $l \approx 30$ lattice sites (root-mean-square width) [42].

Shortly after loading the lattices, we use a 0.17-ms-long clock laser pulse to selectively drive atoms from $|g\uparrow\rangle$ to $|e\uparrow\rangle$. This suddenly introduces a distinct hopping amplitude $t_H \simeq h \times 5$ Hz $\ll t_L$ for the clock state atoms in $|e\uparrow\rangle \equiv |H\rangle$ (heavy). Here, $t_L \simeq h \times 105$ Hz is the unaltered hopping amplitude of the remaining ground-state atoms in $|g\downarrow\rangle \equiv |L\rangle$ (light). The ratio of the hopping amplitudes and the associated mass imbalance is determined by the different lattice depths V_L and $V_H = 3.06(4)V_L$ experienced by $|L\rangle$ and $|H\rangle$ atoms in the SDL [42]. We ensure that the mixture initially remains noninteracting by ramping the magnetic field to the zero crossing of an orbital Feshbach resonance at approximately 1533 G [42,58] before the excitation pulse. Finally, we lower the SDL depth to adjust the hopping ratio t_H/t_L and slowly ramp the magnetic field to 1400–1600 G in accordance with the desired interaction strength. We note that the fraction of doublons as a critical property of the initial state only weakly depends on the chosen interaction parameter [42]. After the state preparation procedure, we translate the minimum of the trapping potential along the tubes by slowly turning on a displaced, state-independent dipole trap, which initiates the transport dynamics. Following the subsequent evolution, we rapidly ramp up the SDL to $V_L \approx 15E_{\mathrm{rec}}$, which freezes the motion of light and heavy atoms. We then turn off the magnetic field and record the density of the light atoms with *in situ* absorption imaging and determine the fraction transported to the new trap minimum [see Fig. 1(b)]. Our imaging intrinsically integrates along one axis of the system, which averages the measurement over an ensemble of tubes with different atom numbers [42].

III. MODEL

Each tube in our experiment is described by a 1D Fermi-Hubbard model with mass imbalance,

$$\hat{\mathcal{H}} = -\sum_{i,\alpha\in\{L,H\}} t_\alpha[\hat{c}^\dagger_{i\alpha}\hat{c}_{(i+1)\alpha} + \text{H.c.}] + U\sum_i \hat{n}_{iL}\hat{n}_{iH} + \frac{\kappa}{2}\sum_{i,\alpha\in\{L,H\}} (i-i_0)^2\hat{n}_{i\alpha}. \quad (1)$$

Here, $\hat{c}_{i\alpha}$ ($\hat{c}^\dagger_{i\alpha}$) denotes the fermionic creation (annihilation) operator for a light ($\alpha = L$) or heavy ($\alpha = H$) atom, $\hat{n}_{i\alpha} \equiv \hat{c}^\dagger_{i\alpha}\hat{c}_{i\alpha}$ the corresponding number operator, t_α the hopping amplitude of each species, and U the on-site interaction. The harmonic confinement is determined by the trap minimum i_0 and strength $\kappa = m\omega^2 d^2 = h \times 3.1(1)$ Hz, with atomic mass m, trapping frequency $\omega = 2\pi \times 40(1)$ Hz, and lattice spacing $d = \lambda/2$.

For a completely frozen heavy species ($t_H = 0$), the Hamiltonian $\hat{\mathcal{H}}$ decouples into single-particle terms for the light species. In this limit, known as the Falicov-Kimball model for $\kappa = 0$ [59], the heavy particles only contribute as an effective binary disorder potential giving rise to single-particle localization [60]. Previous experiments have employed binary mixtures of bosons to probe such a regime, with disorder formed by a fully localized species [61]. In contrast, we study a system of two mobile species with distinct hopping amplitudes $t_L \gg t_H > 0$ [see Fig. 1(c)], realizing two strongly differing but finite scales in the Hamiltonian. For finite interaction strength $|U| > 0$, numerical simulations have suggested that the resulting dynamical constraints can lead to anomalous transport and unconventionally slow thermalization with a nontrivial dependence on the parameters of the model [27,29–32]. At late times, this behavior is expected to be superseded by diffusive transport, as shown in Fig. 1(c). Interestingly, for large interactions and strongly differing masses, the crossover timescale is expected to become extraordinarily large—a genuine many-body effect [42]. In the following measurements, we probe the nature of this transient regime at different times with parameters $t_H/t_L \gtrsim 0.1$ and $|U|/t_L \lesssim 10$.

IV. LOCALIZED SINGLE-PARTICLE STATES

In a first reference measurement, we characterize the single-particle physics originating from the harmonic confinement $\kappa > 0$ in our experiment. It gives rise to single-particle localized eigenstates at the edge of the trap, a phenomenon studied in Refs. [62–67]. These Wannier-Stark-localized states occur because of the finite gradient $\partial_i\hat{\mathcal{H}} = \kappa(i-i_0)\hat{n}_{i\alpha}$ between neighboring lattice sites [68]. To experimentally probe this effect, we prepare a clean sample of noninteracting light atoms by employing a short resonant "push" pulse that removes all $|g\uparrow\rangle$ atoms. Subsequently, we measure the response to a linear translation of the trap minimum as shown in Fig. 1(b). Here, the trap minimum is displaced by $\Delta x/d = i_1 - i_0 = 47(3)$ within time $90(5)\hbar/t_L$, and we consider variable κ/t_L by adjusting the SDL depth in the range $0.69(3)$–$11.8(5)E_{\text{rec}}$.

For all finite lattice depths, we observe a separation of the atoms into two clouds, one close to the initial trap minimum i_0 and one at the final trap minimum i_1, as visible in the insets of Fig. 2(a). We quantify this by determining the number of atoms in the right half of the system N_r, which corresponds to $i \geq i_0 + \Delta x/(2d)$, and compare it to the total number of atoms N. When measuring N_r before the displacement of the trap minimum, we find a nearly constant value of approximately 10%, which we attribute to our finite imaging resolution and a small extent of the initial cloud into the counting region. In Fig. 2(a), we plot the fraction of transported atoms, N_r/N, which is exponentially suppressed for increasing confinement strength. This significant reduction of mass transport in the system results from the properties of the single-particle eigenstates, which are visualized in Fig. 2(b). In general, eigenstates with energies $E_n \in [-2t_L, 2t_L]$ are delocalized across the trap with a nonzero probability density at the center. This behavior changes dramatically for energies $E_n > 2t_L$ corresponding to localized states, in which atoms cannot

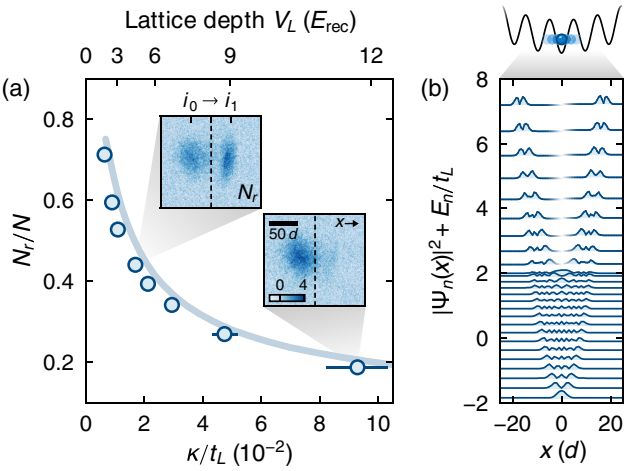

FIG. 2. Wannier-Stark localization in the absence of interactions. (a) Fraction of light atoms N_r/N transported to the right half of the system (blue circles) in the absence of heavy atoms and for variable confinement κ/t_L determined by the lattice depth V_L. Each point is the average of 2–5 measurements, and error bars indicate the uncertainty of κ/t_L (partly smaller than the marker size). The solid line corresponds to our numerical calculation [42], and the insets show raw atomic column densities for $\kappa/t_L = 1.7(1) \times 10^{-2}$ and $9(1) \times 10^{-2}$ with the dashed lines indicating the boundary that determines the atom count N_r in the right half of the system. (b) Probability density $|\Psi_n(x)|^2$ and eigenenergy E_n/t_L of the lowest-lying single-particle eigenstates for $V_L = 9E_{\text{rec}}$ ($\kappa/t_L = 4.9 \times 10^{-2}$). We add a small linear potential to lift the degeneracy of the localized states.

efficiently follow the displaced trap minimum. Crucially, the number of states with $E_n \leq 2t_L$ is reduced as we increase κ/t_L, and therefore, a larger number of localized states becomes occupied in each tube. This explains the observed suppression of N_r/N, which we also reproduce with a theoretical calculation [42] of the experimental protocol [see Fig. 2(a)].

V. INHIBITED TRANSPORT AT EARLY TIMES

Next, we probe how interactions with the heavy species modify the mobility of the light atoms. For this measurement, we set the interaction strength $U/t_L \in [-20, 5]$, a range accessible via magnetic-field tuning of the orbital Feshbach resonance, and choose the fixed hopping ratio $t_H/t_L \simeq 0.1$ and confinement $\kappa/t_L \simeq 1.7 \times 10^{-2}$ by ramping the SDL to $4.7(2)E_{\mathrm{rec}}$. Here, the confinement $\kappa/t_H \simeq 10\kappa/t_L = 1.7 \times 10^{-1}$ suggests that most heavy atoms occupy single-particle localized states according to our previous measurement in the noninteracting regime [see Fig. 2(a)]. However, in the presence of interactions, several of these states delocalize in analogy to the suggested critical gradient required for localization of the interacting Wannier-Stark ladder [63,69–72]. We numerically verify this for our mass-imbalanced case and finite but weak interactions. Here, we find a central trap region of approximately 30 lattice sites, in which the heavy atoms already become mobile during state preparation [42]. Thus, a significant fraction of the system will be responsive to the displacement of the trap potential.

In analogy to our first measurement, we again determine the fraction of transported atoms after displacing the trap minimum by $47(3)d$ within time $92(5)\hbar/t_L$. As we increase the interaction strength $|U|/t_L$, we find a substantial reduction of the transported fraction N_r/N up to a factor of 2 compared to $U = 0$ (see Fig. 3). The behavior for attractive ($U < 0$) and repulsive ($U > 0$) interactions is almost identical, resulting from a similar initial state [42] and the dynamical symmetry of our model in the limit $\kappa = 0$ [73]. We find that the most significant change in the fraction of transported atoms occurs for interaction energies $|U|/t_L < 2$, whereas the signal saturates and remains nearly constant at a low value for $|U|/t_L > 4$. To support our experimental data, we perform matrix-product-state simulations for the Fermi-Hubbard model described in Eq. (1) and a simplified version of the experimental protocol [42]. As shown in the inset of Fig. 3, the extracted N_r/N curve agrees qualitatively with the experiment. Quantitative disagreement is expected due to the significantly lower atom number in the simulation, $\mathcal{N}_{\mathrm{sim}} = 5 \ll \mathcal{N}$.

In our measurement, the apparent suppression of transport results from the constraints in the dynamics of the light atoms arising from interactions with the heavy species, as explored in Fig. 1(c). We emphasize that this measurement primarily probes the early-time dynamics on the timescale $\hbar/t_H$ since the system is effectively frozen and fully separated towards the end of the gradual displacement over the relatively large distance $\Delta x/d \simeq 47$, which exceeds the typical system size $l \approx 30$ (see bottom panels of Fig. 3).

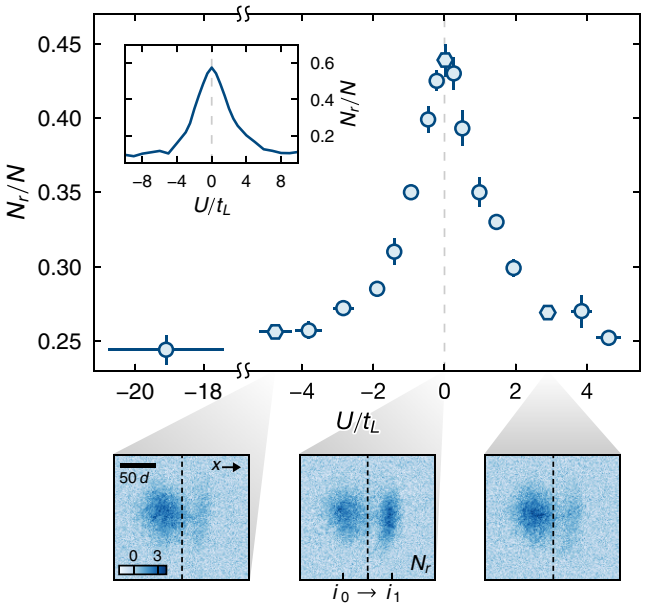

FIG. 3. Constrained early-time dynamics in the interacting heavy-light mixture. Fraction of light atoms N_r/N transported to the right half of the system (blue markers) for variable heavy-light interaction strength U, fixed hopping ratio $t_H/t_L = 0.104(7)$, and confinement $\kappa/t_L = 1.7(1) \times 10^{-2}$. Each point is the average of 3–4 measurements, and error bars (partly smaller than the marker size) denote the standard error of the mean of N_r/N and the uncertainty of U/t_L. The bottom panels show raw atomic column densities for $U/t_L = -4.8(4)$, 0.02(4), and 2.9(2) (from left to right, hexagonal markers), with the dashed lines indicating the boundary that determines the atom count N_r in the right half of the system. The inset of the main panel shows the numerical matrix-product-state simulations of a single tube with the Hubbard parameters and confinement strength of the experiment, and $\mathcal{N}_{\mathrm{sim}} = 5$ atoms of each species.

VI. SLOW RELAXATION AT LATE TIMES

We now turn to the dynamical response of the heavy-light mixture and investigate whether light atoms, remaining close to their initial position during the trap translation, relax towards the final trap minimum at much later times. Such dynamics lead to signatures in the *in situ* density, which we systematically record for a variable hold time. Here, we reduce the displacement to $\Delta x/d \simeq 20 < l$ while keeping the speed of approximately $0.5d(t_L/\hbar)$ unchanged to ensure that the system remains connected and a significant fraction of the heavy atoms are mobile over the traversed distance. The relaxation dynamics can be captured by quantifying the change of the *in situ* density distribution between the initial state after the translation of the trap minimum at a hold time $\tau = 0$ and later times

$0 < \tau \lesssim 400\hbar/t_L$. To this end, we introduce the density deviation observable,

$$\delta n(\tau) = \left\{ \int dx n(x,\tau)[n(x,\tau) - n(x,0)]^2 \right\}^{(1/2)}, \quad (2)$$

which is obtained from the density of the light atoms integrated perpendicularly to the transport direction x and normalized such that $\int dx n(x,\tau) = 1$. For a slow relaxation of the density, this observable grows monotonously with increasing τ, whereas a constant $\delta n(\tau)$ indicates a stationary state of the system.

We probe the influence of the interaction strength on the dynamics by measuring the density deviation for $t_H/t_L \simeq 0.1$ and $U/t_L \simeq 0, -2, -10$, as shown in Fig. 4(a). First, we focus on the noninteracting time trace with $U/t_L \simeq 0$, which shows transient dynamics of $\delta n(\tau)$ at early times for both hopping ratios. These large-amplitude transients are quickly damped due to contributions from different eigenstates. For later times $\tau \gtrsim 100\hbar/t_L$, the density deviation reaches an almost stationary signal, which we also expect from our numerical calculation.

For finite interaction strengths, we find a contrasting behavior with a monotonously increasing density deviation $\delta n(\tau)$ for $\tau > 0$. In this regime, the integrated atomic densities $n(x,\tau)$ show that the light atoms drift towards the final trap minimum at late times [see panels right of Fig. 4(a)]. To extract the timescale of the associated relaxation dynamics, we fit the experimental data to the function $\delta n(\tau) = a(1 - e^{-\tau/\tau_0}) + c$, with the exponential decay constant τ_0 and parameters a, c. For $U/t_L \simeq -2$, we find good agreement between the fitted function and the experimental data with $\tau_0 = 85(17)\hbar/t_L$. In contrast, for the larger interaction strength $U/t_L \simeq -10$, the fit parameters a and τ_0 take unreasonably large values, yielding a linear curve. Until $\tau \approx 100\hbar/t_L$, the measured density deviation grows far less compared to the case with $U/t_L \simeq -2$. To compare the dynamics for the two interaction strengths, we fit the measured density deviation to a linear curve for early times $\tau \leq 101\hbar/t_L$ [42]. Here, we find the linear slope $2(2) \times 10^{-6} t_L/\hbar$ for $U/t_L \simeq -10$ compared to $13(2) \times 10^{-6} t_L/\hbar$ for $U/t_L \simeq -2$. The significantly smaller linear slope illustrates the emergence of unconventionally slow dynamics for strong interactions.

To demonstrate that the slow relaxation stems from dynamical constraints induced by mass imbalance, we also measure the density deviation for the significantly larger $t_H/t_L = 0.34(3)$. For this value of the hopping ratio, the transient regime of unconventional relaxation is expected to be significantly shorter than for the larger ratio studied previously, as illustrated in Fig. 1(c). By changing the wavelength of the SDL to $\lambda' = 690.1$ nm such that $V_H = 1.97(5)V_L$, we realize parameters closely matching our first measurement, apart from the hopping ratio t_H/t_L [42]. Because of this, the confinement strength $\kappa/t_L \simeq 1.7 \times 10^{-2}$ also remains unchanged, ensuring directly comparable systems, in particular, regarding Wannier-Stark-localized states of light atoms. As shown in Fig. 4(b), for $U/t_L \simeq 0$ and -2, the time-dependent behavior remains largely similar to the previous measurement. However, the

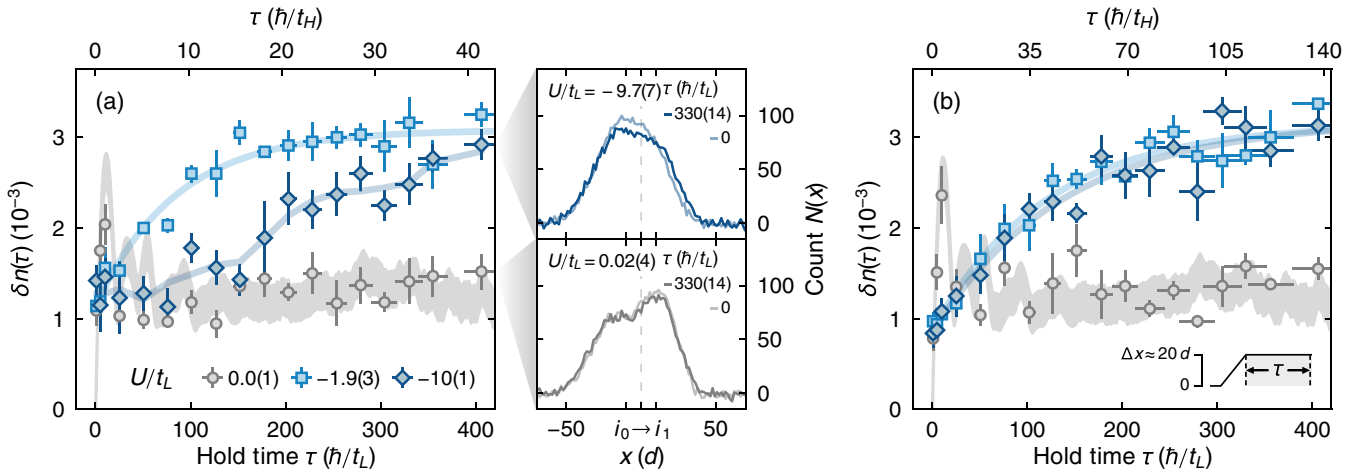

FIG. 4. Late-time relaxation dynamics. Density deviation $\delta n(\tau)$ of the light atoms with respect to the initial atom distribution after translating the trap minimum by Δx [see Eq. (2)], for a variable hold time $\tau > 0$, as illustrated in the bottom-right schematic of panel (b). The time traces correspond to three heavy-light interaction strengths (see legend) with (a) $t_H/t_L = 0.102(6)$ and (b) 0.34(3). Each data point is calculated from the average of 3–5 atomic densities and an independent measurement of $n(x,0)$. Error bars (partly smaller than the marker size) denote the uncertainty of τ, determined from the estimated uncertainty of the hopping amplitude t_L, and standard error of $\delta n(\tau)$, determined from jackknife resampling [42]. The colored lines show exponential fits, as discussed in the main text, and in panel (a), a three-point moving average for $U/t_L \simeq -10$ as a guide to the eye. We show our numerical calculation for $U = 0$ as a gray band, with the height derived from the estimated systematic uncertainty of $\delta n(\tau)$ [42]. The two central panels show integrated atomic densities, which are used to calculate $\delta n(\tau = 330\hbar/t_L)$ in (a).

time trace for $U/t_L \simeq -10$ now only differs negligibly from the one for weaker interactions. From the numerical fit of $\delta n(\tau)$, we extract similar decay constants $\tau_0 = 120(22)\hbar/t_L$ and $138(26)\hbar/t_L$ for the two interaction strengths $U/t_L = -2$ and -10, agreeing with our qualitative observation. The experimental data for $t_H/t_L \simeq 0.3$ confirm a strong dependence of the relaxation dynamics on the interaction strength and mass imbalance between the heavy and light particles. Hence, the unconventionally slow transport emerging in our system can be ascribed to genuine many-body effects.

This observation is further supported by considering the limit of strong interactions and mass imbalances much larger than probed experimentally. In this regime, small-scale numerical calculations predict a pronounced change in the relaxation dynamics of a density modulation, setting in at the timescale $\bar{\tau} \sim \hbar U/t_H^2$ (valid for $U \gg t_L$) [31]. This timescale arises from the collective motion of a bound state comprised of two heavy particles on neighboring sites and a light one delocalized over these sites [27]. However, we find numerical evidence that a noticeable change of dynamics at $\bar{\tau}$ vanishes with increasing system size for moderate hopping ratios $t_H/t_L \geq 0.01$ [42]. These findings are consistent with the experimentally observed relaxation, which does not exhibit prominent features at $\bar{\tau}$. The smooth relaxation dynamics in larger systems could potentially originate from an increased relevance of the many-body medium and a hierarchy of relaxation timescales. Such a hierarchy would emerge from N-body bound states consisting of $(N-1)$ heavy particles and one light particle, only becoming mobile at the timescale $\hbar U t_L^{(N-3)}/t_H^{(N-1)}$.

We briefly comment on how experimental imperfections could also drive the relaxation of $\delta n(\tau)$ in addition to the closed system dynamics of Eq. (1). Most notably, we expect the mobility of the light species to increase from the small loss of heavy atoms, which becomes appreciable for $\tau \gg 100\hbar/t_L$ and reaches up to approximately 20% at $\tau \simeq 400\hbar/t_L$ [42]. However, these losses should be mostly independent of U/t_L since the dominant dissipation process is the off-resonant scattering of SDL photons. By contrast, our data show a strong interaction dependence. Thus, we conclude that the distinct features of the time traces cannot be explained by dissipation.

VII. DISCUSSION AND OUTLOOK

We have characterized the density dynamics of the mass-imbalanced Fermi-Hubbard model after a gradual change of the external trapping potential, which can be summarized as follows. First, our data show relaxation of the density for all finite interaction parameters and hopping ratios at late times. Second, for the strongest interaction $U/t_L \simeq -10$ and smallest hopping ratio $t_H/t_L \simeq 0.1$ probed in our experiment, the system relaxes much slower as a result of the dynamical constraints induced by the heavy species. Comparing this observation to the much faster relaxation for $U/t_L \simeq -2$ shows that the slow, emergent timescale must involve many-body effects. Thus, our experimental platform gives access to a particularly interesting class of unconventionally slow dynamics that exist in the absence of static disorder and can be controlled solely by interactions.

In future experiments, variable-wavelength density modulations could provide an ideal setting to directly study anomalous transport in this system. Moreover, it would be particularly interesting to investigate the effect of integrability on transport in the one-dimensional, mass-balanced, Fermi-Hubbard model and explore the weak breaking of integrability by only slightly detuning the hopping amplitudes of the two species. Our work also motivates the experimental study of transport in other strongly constrained states of quantum matter, which can be found in Rydberg-blockaded systems, strongly tilted lattices, and realizations of lattice gauge theories [19,24,37,38,74,75].

ACKNOWLEDGMENTS

We acknowledge valuable and helpful discussions with Dmitry A. Abanin, Johannes Feldmeier, Sarang Gopalakrishnan, Bharath Hebbe Madhusudhana, Markus Müller, Luis Riegger, Pablo Sala, Sebastian Scherg, and Alessandro Silva, and we are grateful to Jesper Levinsen and Meera M. Parish for helpful insights on the orbital Feshbach resonance in an optical lattice. The authors also wish to thank Alexander Impertro for technical contributions to the experiment. This project has received funding from the Deutsche Forschungsgemeinschaft (DFG, German Research Foundation) under Germany's Excellence Strategy–EXC-2111–390814868, DFG TRR80 and DFG Grant No. KN1254/2-1, the European Research Council (ERC) under the European Union's Horizon 2020 research and innovation programme (Grant Agreement No. 817482 and No. 851161), and the Technical University of Munich–Institute for Advanced Study, funded by the German Excellence Initiative and the European Union FP7 under Grant Agreement No. 291763.

[1] J. M. Deutsch, *Quantum Statistical Mechanics in a Closed System*, Phys. Rev. A **43**, 2046 (1991).
[2] M. Srednicki, *Chaos and Quantum Thermalization*, Phys. Rev. E **50**, 888 (1994).
[3] M. Rigol, V. Dunjko, and M. Olshanii, *Thermalization and Its Mechanism for Generic Isolated Quantum Systems*, Nature (London) **452**, 854 (2008).
[4] L. D'Alessio, Y. Kafri, A. Polkovnikov, and M. Rigol, *From Quantum Chaos and Eigenstate Thermalization to Statistical Mechanics and Thermodynamics*, Adv. Phys. **65**, 239 (2016).
[5] I. Bloch, J. Dalibard, and W. Zwerger, *Many-Body Physics with Ultracold Gases*, Rev. Mod. Phys. **80**, 885 (2008).

[6] R. Blatt and C. F. Roos, *Quantum Simulations with Trapped Ions*, Nat. Phys. **8**, 277 (2012).
[7] M. Kjaergaard, M. E. Schwartz, J. Braumüller, P. Krantz, J. I.-J. Wang, S. Gustavsson, and W. D. Oliver, *Superconducting Qubits: Current State of Play*, Annu. Rev. Condens. Matter Phys. **11**, 369 (2020).
[8] P. C. Hohenberg and B. I. Halperin, *Theory of Dynamic Critical Phenomena*, Rev. Mod. Phys. **49**, 435 (1977).
[9] S. Mukerjee, V. Oganesyan, and D. Huse, *Statistical Theory of Transport by Strongly Interacting Lattice Fermions*, Phys. Rev. B **73**, 035113 (2006).
[10] J. Lux, J. Müller, A. Mitra, and A. Rosch, *Hydrodynamic Long-Time Tails after a Quantum Quench*, Phys. Rev. A **89**, 053608 (2014).
[11] A. Bohrdt, C. B. Mendl, M. Endres, and M. Knap, *Scrambling and Thermalization in a Diffusive Quantum Many-Body System*, New J. Phys. **19**, 063001 (2017).
[12] M. Schreiber, S. S. Hodgman, P. Bordia, H. P. Lüschen, M. H. Fischer, R. Vosk, E. Altman, U. Schneider, and I. Bloch, *Observation of Many-Body Localization of Interacting Fermions in a Quasi-Random Optical Lattice*, Science **349**, 842 (2015).
[13] S. S. Kondov, W. R. McGehee, W. Xu, and B. DeMarco, *Disorder-Induced Localization in a Strongly Correlated Atomic Hubbard Gas*, Phys. Rev. Lett. **114**, 083002 (2015).
[14] J. Smith, A. Lee, P. Richerme, B. Neyenhuis, P. W. Hess, P. Hauke, M. Heyl, D. A. Huse, and C. Monroe, *Many-Body Localization in a Quantum Simulator with Programmable Random Disorder*, Nat. Phys. **12**, 907 (2016).
[15] P. Roushan *et al.*, *Spectroscopic Signatures of Localization with Interacting Photons in Superconducting Qubits*, Science **358**, 1175 (2017).
[16] R. Nandkishore and D. A. Huse, *Many-Body Localization and Thermalization in Quantum Statistical Mechanics*, Annu. Rev. Condens. Matter Phys. **6**, 15 (2015).
[17] D. A. Abanin, E. Altman, I. Bloch, and M. Serbyn, *Colloquium: Many-Body Localization, Thermalization, and Entanglement*, Rev. Mod. Phys. **91**, 021001 (2019).
[18] M. Serbyn, M. Knap, S. Gopalakrishnan, Z. Papić, N. Y. Yao, C. R. Laumann, D. A. Abanin, M. D. Lukin, and E. A. Demler, *Interferometric Probes of Many-Body Localization*, Phys. Rev. Lett. **113**, 147204 (2014).
[19] H. Bernien, S. Schwartz, A. Keesling, H. Levine, A. Omran, H. Pichler, S. Choi, A. Zibrov, M. Endres, M. Greiner, V. Vuletic, and M. D. Lukin, *Probing Many-Body Dynamics on a 51-Atom Quantum Simulator*, Nature (London) **551**, 579 (2017).
[20] C. J. Turner, A. A. Michailidis, D. A. Abanin, M. Serbyn, and Z. Papić, *Weak Ergodicity Breaking from Quantum Many-Body Scars*, Nat. Phys. **14**, 745 (2018).
[21] R. M. Nandkishore and M. Hermele, *Fractons*, Annu. Rev. Condens. Matter Phys. **10**, 295 (2019).
[22] A. Gromov, A. Lucas, and R. M. Nandkishore, *Fracton Hydrodynamics*, Phys. Rev. Research **2**, 033124 (2020).
[23] J. Feldmeier, P. Sala, G. De Tomasi, F. Pollmann, and M. Knap, *Anomalous Diffusion in Dipole- and Higher-Moment-Conserving Systems*, Phys. Rev. Lett. **125**, 245303 (2020).
[24] E. Guardado-Sanchez, A. Morningstar, B. M. Spar, P. T. Brown, D. A. Huse, and W. S. Bakr, *Subdiffusion and Heat Transport in a Tilted Two-Dimensional Fermi-Hubbard System*, Phys. Rev. X **10**, 011042 (2020).
[25] Yu. Kagan and L. A. Maksimov, *Localization in a Subsystem of Interacting Particles Diffusing in a Regular Crystal*, J. Exp. Theor. Phys. **60**, 201 (1984).
[26] W. De Roeck and F. Huveneers, *Asymptotic Quantum Many-Body Localization from Thermal Disorder*, Commun. Math. Phys. **332**, 1017 (2014).
[27] M. Schiulaz and M. Müller, *Ideal Quantum Glass Transitions: Many-Body Localization without Quenched Disorder*, AIP Conf. Proc. **1610**, 11 (2014).
[28] M. Schiulaz, A. Silva, and M. Müller, *Dynamics in Many-Body Localized Quantum Systems without Disorder*, Phys. Rev. B **91**, 184202 (2015).
[29] W. De Roeck and F. Huveneers, *Scenario for Delocalization in Translation-Invariant Systems*, Phys. Rev. B **90**, 165137 (2014).
[30] Z. Papić, E. M. Stoudenmire, and D. A. Abanin, *Many-Body Localization in Disorder-Free Systems: The Importance of Finite-Size Constraints*, Ann. Phys. (Amsterdam) **362**, 714 (2015).
[31] N. Y. Yao, C. R. Laumann, J. I. Cirac, M. D. Lukin, and J. E. Moore, *Quasi-Many-Body Localization in Translation-Invariant Systems*, Phys. Rev. Lett. **117**, 240601 (2016).
[32] J. Sirker, *Exploration of the Existence of a Distinct Quasi Many-Body Localized Phase: Numerical Study of a Translationally Invariant System in the Thermodynamic Limit*, Phys. Rev. B **99**, 075162 (2019).
[33] Z. Lan, M. van Horssen, S. Powell, and J. P. Garrahan, *Quantum Slow Relaxation and Metastability due to Dynamical Constraints*, Phys. Rev. Lett. **121**, 040603 (2018).
[34] J. Feldmeier, F. Pollmann, and M. Knap, *Emergent Glassy Dynamics in a Quantum Dimer Model*, Phys. Rev. Lett. **123**, 040601 (2019).
[35] N. Pancotti, G. Giudice, J. I. Cirac, J. P. Garrahan, and M. C. Bañuls, *Quantum East Model: Localization, Nonthermal Eigenstates, and Slow Dynamics*, Phys. Rev. X **10**, 021051 (2020).
[36] E. Guardado-Sanchez, B. M. Spar, P. Schauss, R. Belyansky, J. T. Young, P. Bienias, A. V. Gorshkov, T. Iadecola, and W. S. Bakr, *Quench Dynamics of a Fermi Gas with Strong Nonlocal Interactions*, Phys. Rev. X **11**, 021036 (2021).
[37] S. Scherg, T. Kohlert, P. Sala, F. Pollmann, B. Hebbe Madhusudhana, I. Bloch, and M. Aidelsburger, *Observing Non-ergodicity due to Kinetic Constraints in Tilted Fermi-Hubbard Chains*, Nat. Commun. **12**, 4490 (2021).
[38] W. Morong, F. Liu, P. Becker, K. S. Collins, L. Feng, A. Kyprianidis, G. Pagano, T. You, A. V. Gorshkov, and C. Monroe, *Observation of Stark Many-Body Localization without Disorder*, Nature (London) **599**, 393 (2021).
[39] A. D. Ludlow, M. M. Boyd, J. Ye, E. Peik, and P. O. Schmidt, *Optical Atomic Clocks*, Rev. Mod. Phys. **87**, 637 (2015).
[40] L. Riegger, N. Darkwah Oppong, M. Höfer, D. R. Fernandes, I. Bloch, and S. Fölling, *Localized Magnetic Moments with Tunable Spin Exchange in a Gas of Ultracold Fermions*, Phys. Rev. Lett. **120**, 143601 (2018).
[41] Z. W. Barber, J. E. Stalnaker, N. D. Lemke, N. Poli, C. W. Oates, T. M. Fortier, S. A. Diddams, L. Hollberg,

C. W. Hoyt, A. V. Taichenachev, and V. I. Yudin, *Optical Lattice Induced Light Shifts in an Yb Atomic Clock*, Phys. Rev. Lett. **100**, 103002 (2008).

[42] See Supplemental Material http://link.aps.org/supplemental/10.1103/PhysRevX.12.031026, which includes Refs. [43–57], for additional information about the experimental methods and a detailed discussion of the numerical simulations.

[43] M. Kitagawa, K. Enomoto, K. Kasa, Y. Takahashi, R. Ciuryło, P. Naidon, and P. S. Julienne, *Two-Color Photoassociation Spectroscopy of Ytterbium Atoms and the Precise Determinations of s-Wave Scattering Lengths*, Phys. Rev. A **77**, 012719 (2008).

[44] M. Köhl, *Thermometry of Fermionic Atoms in an Optical Lattice*, Phys. Rev. A **73**, 031601(R) (2006).

[45] N. Darkwah Oppong, L. Riegger, O. Bettermann, M. Höfer, J. Levinsen, M. M. Parish, I. Bloch, and S. Fölling, *Observation of Coherent Multiorbital Polarons in a Two-Dimensional Fermi Gas*, Phys. Rev. Lett. **122**, 193604 (2019).

[46] S. Friebel, C. D'Andrea, J. Walz, M. Weitz, and T. W. Hänsch, CO_2*-Laser Optical Lattice with Cold Rubidium Atoms*, Phys. Rev. A **57**, R20 (1998).

[47] C. Chin, R. Grimm, P. Julienne, and E. Tiesinga, *Feshbach Resonances in Ultracold Gases*, Rev. Mod. Phys. **82**, 1225 (2010).

[48] E. K. Laird, Z.-Y. Shi, M. M. Parish, and J. Levinsen, *Frustrated Orbital Feshbach Resonances in a Fermi Gas*, Phys. Rev. A **101**, 022707 (2020).

[49] F. Verstraete, J. J. García-Ripoll, and J. I. Cirac, *Matrix Product Density Operators: Simulation of Finite-Temperature and Dissipative Systems*, Phys. Rev. Lett. **93**, 207204 (2004).

[50] M. Zwolak and G. Vidal, *Mixed-State Dynamics in One-Dimensional Quantum Lattice Systems: A Time-Dependent Superoperator Renormalization Algorithm*, Phys. Rev. Lett. **93**, 207205 (2004).

[51] J. Hauschild and F. Pollmann, *Efficient Numerical Simulations with Tensor Networks: Tensor Network Python (TeNPy)*, SciPost Phys. Lect. Notes **5** (2018).

[52] S. Paeckel, T. Köhler, A. Swoboda, S. R. Manmana, U. Schollwöck, and C. Hubig, *Time-Evolution Methods for Matrix-Product States*, Ann. Phys. (Amsterdam) **411**, 167998 (2019).

[53] G. Vidal, *Efficient Simulation of One-Dimensional Quantum Many-Body Systems*, Phys. Rev. Lett. **93**, 040502 (2004).

[54] R. Sensarma, D. Pekker, E. Altman, E. Demler, N. Strohmaier, D. Greif, R. Jördens, L. Tarruell, H. Moritz, and T. Esslinger, *Lifetime of Double Occupancies in the Fermi-Hubbard Model*, Phys. Rev. B **82**, 224302 (2010).

[55] A. Auerbach, *Interacting Electrons and Quantum Magnetism* (Springer, New York, 1994).

[56] B. Bertini, F. Heidrich-Meisner, C. Karrasch, T. Prosen, R. Steinigeweg, and M. Žnidarič, *Finite-Temperature Transport in One-Dimensional Quantum Lattice Models*, Rev. Mod. Phys. **93**, 025003 (2021).

[57] B. Efron and C. Stein, *The Jackknife Estimate of Variance*, Ann. Stat. **9**, 586 (1981).

[58] O. Bettermann, N. Darkwah Oppong, G. Pasqualetti, L. Riegger, I. Bloch, and S. Fölling, *Clock-Line Photoassociation of Strongly Bound Dimers in a Magic-Wavelength Lattice*, arXiv:2003.10599.

[59] L. M. Falicov and J. C. Kimball, *Simple Model for Semiconductor-Metal Transitions:* SmB_6 *and Transition-Metal Oxides*, Phys. Rev. Lett. **22**, 997 (1969).

[60] T. Heitmann, J. Richter, T. Dahm, and R. Steinigeweg, *Density Dynamics in the Mass-Imbalanced Hubbard Chain*, Phys. Rev. B **102**, 045137 (2020).

[61] B. Gadway, D. Pertot, J. Reeves, M. Vogt, and D. Schneble, *Glassy Behavior in a Binary Atomic Mixture*, Phys. Rev. Lett. **107**, 145306 (2011).

[62] L. Pezzè, L. Pitaevskii, A. Smerzi, S. Stringari, G. Modugno, E. de Mirandes, F. Ferlaino, H. Ott, G. Roati, and M. Inguscio, *Insulating Behavior of a Trapped Ideal Fermi Gas*, Phys. Rev. Lett. **93**, 120401 (2004).

[63] H. Ott, E. de Mirandes, F. Ferlaino, G. Roati, G. Modugno, and M. Inguscio, *Collisionally Induced Transport in Periodic Potentials*, Phys. Rev. Lett. **92**, 160601 (2004).

[64] G. Orso, L. P. Pitaevskii, and S. Stringari, *Umklapp Collisions and Center-of-Mass Oscillations of a Trapped Fermi Gas*, Phys. Rev. Lett. **93**, 020404 (2004).

[65] M. Rigol and A. Muramatsu, *Confinement Control by Optical Lattices*, Phys. Rev. A **70**, 043627 (2004).

[66] A. M. Rey, G. Pupillo, C. W. Clark, and C. J. Williams, *Ultracold Atoms Confined in an Optical Lattice Plus Parabolic Potential: A Closed-Form Approach*, Phys. Rev. A **72**, 033616 (2005).

[67] M. Schulz, C. A. Hooley, and R. Moessner, *Slow Relaxation and Sensitivity to Disorder in Trapped Lattice Fermions after a Quench*, Phys. Rev. A **94**, 063643 (2016).

[68] G. H. Wannier, *Dynamics of Band Electrons in Electric and Magnetic Fields*, Rev. Mod. Phys. **34**, 645 (1962).

[69] N. Strohmaier, Y. Takasu, K. Günter, R. Jördens, M. Köhl, H. Moritz, and T. Esslinger, *Interaction-Controlled Transport of an Ultracold Fermi Gas*, Phys. Rev. Lett. **99**, 220601 (2007).

[70] M. Schulz, C. A. Hooley, R. Moessner, and F. Pollmann, *Stark Many-Body Localization*, Phys. Rev. Lett. **122**, 040606 (2019).

[71] E. van Nieuwenburg, Y. Baum, and G. Refael, *From Bloch Oscillations to Many-Body Localization in Clean Interacting Systems*, Proc. Natl. Acad. Sci. U.S.A. **116**, 9269 (2019).

[72] T. Chanda, R. Yao, and J. Zakrzewski, *Coexistence of Localized and Extended Phases: Many-Body Localization in a Harmonic Trap*, Phys. Rev. Research **2**, 032039(R) (2020).

[73] U. Schneider, L. Hackermüller, J. P. Ronzheimer, S. Will, S. Braun, T. Best, I. Bloch, E. Demler, S. Mandt, D. Rasch, and A. Rosch, *Fermionic Transport and Out-of-Equilibrium Dynamics in a Homogeneous Hubbard Model with Ultracold Atoms*, Nat. Phys. **8**, 213 (2012).

[74] E. A. Martinez, C. A. Muschik, P. Schindler, D. Nigg, A. Erhard, M. Heyl, P. Hauke, M. Dalmonte, T. Monz, P. Zoller, and R. Blatt, *Real-Time Dynamics of Lattice Gauge Theories with a Few-Qubit Quantum Computer*, Nature (London) **534**, 516 (2016).

[75] B. Yang, H. Sun, R. Ott, H.-Y. Wang, T. V. Zache, J. C. Halimeh, Z.-S. Yuan, P. Hauke, and J.-W. Pan, *Observation of Gauge Invariance in a 71-Site Bose–Hubbard Quantum Simulator*, Nature (London) **587**, 392 (2020).